INTL JOURNAL OF ELECTRONICS AND TELECOMMUNICATIONS, 2026, VOL. 72, NO. 2, PP. 1-10
Manuscript received January 28, 2026; revised April 2026. doi: 10.24425/ijet.2026.157925

Hybrid optical–acoustic underwater communication with joint modulation and bio-inspired power optimization

Lenin Joseph, and Sangeetha Anandan

***Abstract*—A hybrid optical–acoustic underwater wireless communication system that integrates optical links at short ranges and acoustic links in long ranges for high bandwidth underwater applications is presented in our work. The system utilizes optical intra-cluster and acoustic inter-cluster links, with cooperative communication to improve data transmission and reliability. Analytical models incorporating acoustic and optical signal attenuation and noise are developed, considering practical underwater conditions. Optical links utilize Quadrature Amplitude Modulation with Turbo coding, while acoustic links adopt Frequency Shift Keying with Reed–Solomon coding to ensure reliable data transmission under heterogeneous channel conditions. Simulations demonstrate that the proposed framework supports robust transmission under different propagation conditions in an underwater environment. Furthermore, a bio inspired power optimization algorithm reduces transmission power consumption while maintaining stable throughput and received traffic load.**

***Keywords*—Underwater wireless communication; cooperative communication; hybrid optical–acoustic; optimization algorithm**

I. Introduction

DESPITE extensive advancements in communication technologies, achieving reliable and efficient underwater communication is a significant challenge compared to its terrestrial counterpart. Over the past decades, researchers have worked to realise stable underwater wireless communication (UWC) systems [1]. However, there are several significant and distinct challenges in achieving consistent UWC because of the aquatic medium's intrinsic characteristics and highly dynamic nature [2]. Terrestrial radio frequency (RF) systems are also not practical in underwater environments because of the high attenuation in water, which is exacerbated in conductive ocean water. Severe energy constraints are also a major issue with wireless communication in the underwater environment. Underwater nodes must continue to function for the duration of their mission, which lasts for days, months, or even years, despite having limited battery energy storage. It is expensive and challenging to recharge or replace the batteries in these nodes. To address these issues, researchers have created alternative physical layer technologies such as underwater acoustic communication (UAC), underwater optical communication (UOC), and underwater magnetic induction communication (UMIC). Each of these strategies has merits and demerits. UAC is used for long-distance communication, but it has low bandwidth, low speed, high energy consumption, and multipath problems. In comparison to UAC and UMIC, UOC provides high-speed, high-bandwidth, low-power communication at the trade-off of poorer dependability and shorter range. Internet of Underwater Things (IoUT) is the result of the explosion of academic, commercial, and defense interest in the UWC field brought about by the introduction of these new technologies [3],[4],[5]. However, because IoUT includes a diverse set of applications with varying network performance requirements, a single communication technology is insufficient to meet its aims [6], [7]. UWC networks face challenges due to the limits of existing technologies, such as acoustic and optical systems, which either consume too much power or have a limited communication range [8][9]. These restrictions are especially significant considering the changing undersea conditions and data flow. Current UWC systems frequently lack energy-efficient techniques capable of responding to changing environmental and operational demands. Thus, establishing an optimum power-efficient, communication technique for such cases is critical [10].

To address above stated limitations of UWC and UAC, hybrid optical–acoustic communication frameworks have been proposed thereby to exploit the complementary strengths of optical and acoustic technologies [9].

Our proposed work discusses a hybrid optical-acoustic underwater wireless communication framework that incorporates cooperative transmission, practical channel modeling, joint modulation with coding schemes, and energy-efficient power optimization [11]. Transmission power is optimized using a bio inspired algorithm named Electric Eel Foraging Optimization algorithm (EEFOA) [27]. The overall contributions of this paper are summarized as follows.

- A hybrid underwater wireless communication framework is proposed, combining optical intra-cluster links and acoustic inter-cluster links to improve reliability and coverage under varying underwater conditions.
- Practical analytical models are incorporated to characterize underwater optical and acoustic attenuation and noise, enabling realistic performance evaluation under stochastic channel conditions.
- A hybrid physical-layer transmission scheme is adopted, employing quadrature amplitude modulation (QAM) with Turbo coding for optical links and frequency shift keying (FSK) with Reed–Solomon (RS) coding for acoustic links to enhance reliability across bandwidth and noise constrained channels.
- An energy-efficient transmission power allocation strategy based on the EEFO algorithm is applied to

Authors are with VIT University, Vellore, India (email-leninzmail@gmail.com; asangeetha@vit.ac.in).

minimize energy consumption while maintaining throughput requirements.

II. Related works

Several research studies in literature have explored hybrid optical-acoustic transmission techniques; a few of those works are reviewed here.

In 2024, Zhu, W., et.al [1] has proposed an approach that uses a hybrid technique, transmitting higher importance data using optical waves, lower importance data using acoustic waves. The presented method lowers packet loss in vacant regions, increasing packet delivery rate (PDR).

In 2023, Angara, B.R., et.al [12] has presented channel modeling using bubbles from the ocean. Uplink UWOC system with particles and bubbles at different wind speeds were investigated. Simulations were performed utilizing optical characteristics of underwater to compute connection lengths and signal loss between the UWOC system transmitter as well as receiver. The power on reception was determined using different configurations of the receiver and oceanic conditions, with and without bubbles.

TABLE I
COMPARISON OF RELATED WORKS

Reference	Models	Merits	Demerits
[1]	Routing Protocol for Hybrid WSN	Reduces packet loss in void zones	Introduces high routing overhead
[12]	Channel modeling with oceanic bubbles	Improves accuracy of environmental modeling	Performance varies with ocean conditions
[13]	Real-time High-Speed UOWC Deployment	Supports long-term, stable communication	High system deployment cost
[14]	OCDMA Transmission	Allows simultaneous multi-user access	Complex system synchronization

In 2023, Zhang, J., et.al [13] have demonstrated high speed UWOC in the deep sea that are both real-time and long-term. With bitrates of up to 125 Mbps, it was the first deep-sea UWOC link to operate continuously for an extended period. A high-quality transmission of video signals was accomplished, and it has demonstrated the capacity of their system to transport such high-quality films lossless.

In 2023, El-Mottaleb, S.A.A., et.al [14] has presented an optical code division multiple access (OCDMA) transmission-dependent UWC system. The permutation vector code was used to describe a scheme using OCDMA transmission.

Recent investigations from literature have demonstrated that classical Rayleigh or Rician models don't always effectively trace the statistics of underwater acoustic or optical channels, especially in the presence of shadowing, turbulence and non-stationary environments. The results from measurement-based models shows that k–μ shadowed, Weibull, generalized Gamma and mixed distributions give a much better fitting to the underwater acoustic propagation channel compared to the statistical distributions like log normal (LN), Gamma- Gamma (GG), generalized Gamma or Weibull for the turbulence induce fading in that of optical model. However, in our work, we choose to characterize the underwater link fading by a LN distribution because the shallow-water channels generally display log-normal statistics for large-scale gain and small-scale amplitude fluctuation under mild scattering and shadowing conditions. Table II shows a comparison of fading models.

TABLE II
COMPARISON OF FADING MODELS

Model type	Examples	Typical use
Additive white Gaussian Noise (AWGN)	AWGN	Ideal / upper bound
Small scale fading	Rayleigh, Rician, Nakagami-m	Basic underwater links
Shadowing	Lognormal	Large-scale obstruction effects
Composite models	Rayleigh + Log normal, k-μ shadowed, Gamma/Gamma	Realistic channel modeling
Generalized models	α-μ, k-μ, η-μ, Generalized-Gamma	Fitting detailed measurements

In their work, Busacca et. al study predictive channel models for actual shallow-water acoustic settings, emphasizing the channel's non-stationarity and temporal unpredictability [28]. Further, in 2025, Ghosh et. al stated that more sophisticated fading patterns can be captured by generalized distributions as k–μ shadowing, especially in circumstances associated by Reconfigurable Hybrid Surfaces (RIS) [29]. In their publications from 2025, Li et. al and Haziq et. al highlight that as underwater acoustic and specifically hybrid links are significantly impacted by fading, turbulence, and Doppler, and that suitable channel models are essential for accurate performance analysis [30]. Considering this recent research, we understand that the LN model we adopted is a simplified representation and that more general fading distributions may be required in harsher or highly non-stationary environments and a full comparative fitting study against the channel fading distribution models is left for future work.

III. System Model

The proposed model consists of clustered underwater nodes. Cooperative transmission is adopted to improve reliability and traffic handling capability. Depending on the requirements and link availability the nodes can make dynamic switching between optical and acoustic links. At first, a network model and then a traffic model is created for our proposed system. Further, analytical models are developed to calculate the losses in both the channels [11].

A. Network Model

The hybrid opto-acoustic UWCN scheme is represented in Figure 1. The proposed technique consists of B nodes, with a base station and M-1 nodes (m=1, 2…M). Nodes are grouped in $N_{Cluster}$, as denoted as n=1,2,....,$N_{cluster.}$ For each cluster, the topology varies. Member Nodes (MNs) in each cluster communicate with Cluster Heads (CHs) utilizing higher speed, lower power and short-range optical links. MN includes sensor nodes, AUVs, Remotely Operated Vehicle (ROV). After collecting data from MNs, CHs use hybrid opto-acoustic links to relay-to-relay Node (RN) or Base Station (BS), Surface Sink (SS), based on traffic demand, weather. BS/SS are linked to on-shore ground control, including satellites utilizing over-the-air (OTA) RF links. We follow the network given in [11] to frame our model.

B. Traffic Model

As considered in the model given in [11], a constant bit rate (CBR), a variable bit rate (VBR) and a best effort (BE) traffic types are considered. Hourly traffic flow is considered over 7 days. These data match to various IoUT applications discussed above, which produce varied traffic demands. Underwater sensors are utilized for scientific temperature, pH, and salinity measurements with low data rates. Figure 2 represents the spatial 3D distribution of nodes within the three clusters in the network topology. Each node is represented by its (X, Y, Z) coordinates and a cluster label (e.g., 0, 1, or 2) with its number of nodes given as N. Figure 3 depicts the 2D spatial layout and propagation of nodes across the three network clusters [11].

Over the data collection period, the traffic load demonstrates notable fluctuations. Traffic is predominantly concentrated within the optical distance range of 10 to 70 meters, where dense variations in load are observed, reaching up to 8 units.

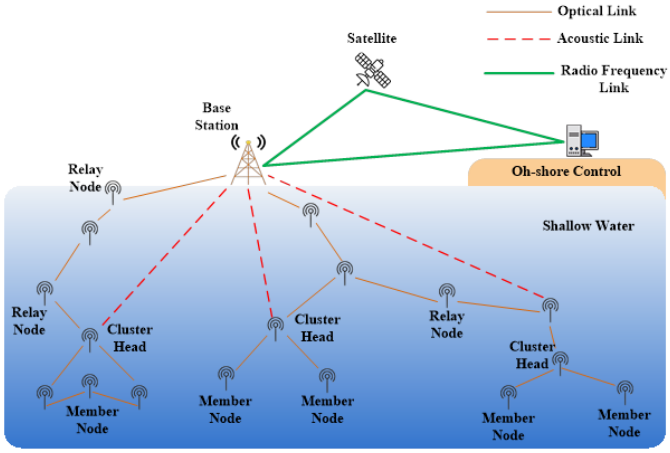

Fig. 1. The network model

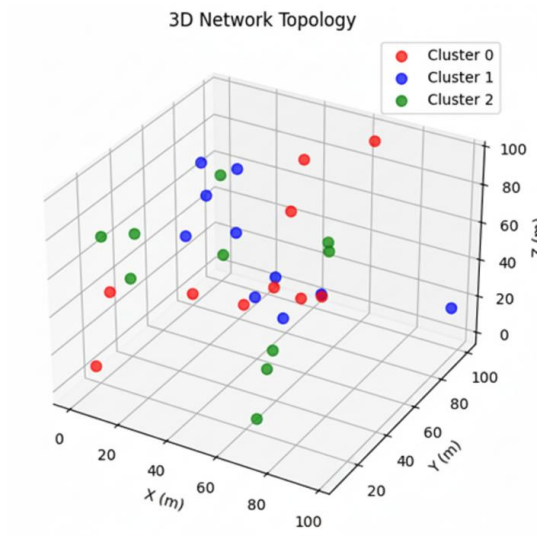

Fig. 2. 3D network topology showing node distribution across 3 clusters

C. Acoustic Channel Propagation Model

An analytical model created for UAC channel propagation depending on the networks is described in [11]. Total route loss of UAC through absorption and spreading is shown in equation (1).

$$S_{ac}(f,g) = S_0 \cdot f^k \cdot \alpha_{ac}(g)^{f_{km}} \quad (1)$$

Here, the term S_0 accounts for normalization factor (NF) refers to inverse of transmitted power, f^k implies spreading loss distance $f(m)$ among transmitter as well as receiver, k implies path loss exponent and term $\alpha_{ac}(g)^{f_{km}}$ implies absorption coefficient (dB/km) accounts of absorption loss distance $f_{km} = f \times 10^{-3}$given in km.

Total UAC path loss in dB is given in equation (2).

$$10\,log\,S_{ac}\,(f,g) = 10\,log\,S_0 + k \cdot 10\,log\,f + f_{km} \cdot 10\,log\,\alpha_{ac}(g) \quad (2)$$

Absorption coefficient $10\,log\,\alpha_{ac}(g)$ of acoustic signal frequency function g and water salinity function S, water pH, water temperature T, depth of water z and acoustic speed of propagation v_{ac} is given using equation (3).

$$v_{ac} = 1412 + 3.21\,T + 1.19\,S + 0.0167z \quad (3)$$

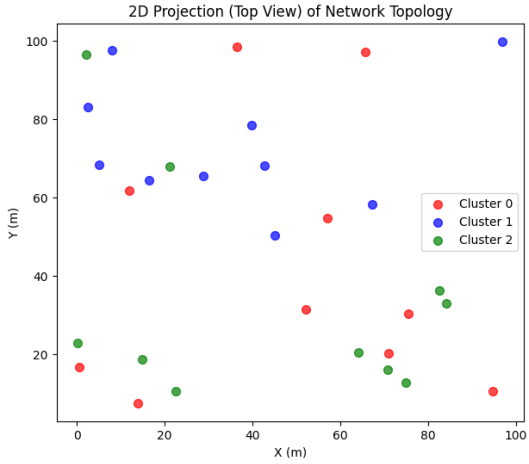

Fig. 3. 2D propagation view of network topology with 3 clusters

The literature provides numerous formulae [16],[17] of obtaining absorption coefficient $10\,log\,\alpha_{ac}(g)$. Thorps empirical formula is the commonly used model. Thorp's statement is limited to lower water temperatures and does not account for factors such as salinity, pressure, temperature, speed of sound, depth. Thorp's formula is derived from measurements in standard oceanic environments. The conditions include around 4°C temperature, a salinity of approximately 35 parts per thousand, and a depth of about 1000 meters. It gives accurate results under these oceanic conditions typically for acoustic applications. However, in environments with significantly different temperatures, salinity, or pH, where absorption mechanisms have harsh variations, Thorp's formula has its limitations. Therefore, when applying this formula, its limitations must be considered.

The appropriate technique encapsulates oceanic factors within the frequency range $100Hz < g < 1MHz$ as expressed by equation (4), proposed by Francois and Garrison in 1982.

$$\alpha(g) = \frac{S_1 Q_1 g_1 g^2}{g^2+g_1^2} + \frac{S_2 Q_2 g_2 g^2}{g^2+g_2^2} + S_3 Q_3 g^2 \quad (4)$$

Here, three terms are associated, in which term 1 is created using the Boric acid (H_3BO_3) molecules to account the effect of ironic relaxation. Term 2 is related to effects created by magnesium sulphate salts ($MgSO_4$) and term 3 explains component of absorption caused by pure water.

D. Acoustic Noise Model

UAC is susceptible to a range of underwater noise sources in addition to attenuation issues. Ambient underwater noise impacting water acoustics is classed depending on the frequency range where its effects are most noticeable. Based on the research [11], a general ambient noise model is estimated from typical noise sources utilizing Gaussian statistics and continuous power spectral density. Noise sources are outlined below.

1) Turbulence Noise $M_t(g)$- This is related to the turbulence of oceanic wave. The noise is noticeable in g<10 Hz range and given in equation (5). Here, g denotes the frequency variable in Hertz.

$$10\,log\,M_t\,(g) = 17 - 30\,log\,g \tag{5}$$

2) Shipping/Vessel Noise $M_s(g)$- This noise is produced by a shipping or a vessel in water, dominant within 10<g<100 Hz band and formulated in equation (6).

$$10\,log\,M_s\,(g) = 40 + 20(s - 0.5) + 26\,log\,g - 60\,log(g + 0.03) \tag{6}$$

Here, s∈[0,1] implies shipping factors.

3)Wave noise $M_w(g)$- This includes the noise generated by the wind on the surface of water and noticeable in $100\ Hz < g < 100\ kHz$ range. The noise component is represented in equation (7).

$$10\,log\,M_w\,(g) = 50 + 7.5\sqrt{w_s} + 20\,log\,g - 40\,log(g + 0.4) \tag{7}$$

Here, w_s represents wind speeds in m/s.

4)Thermal noise $M_{th}(g)$- The frequency range occurs above $g > 100\ kHz$ on account of thermal agitation through ocean pressure variations. It gives a lower bound of ambient noise levels in the ocean expressed in equation (8).

$$10\,log\,M_{th}\,(g) = -15 + 20\,log\,g \tag{8}$$

Total noise Power Spectral Density (PSD) $M_{total}(g)$ is given below.

$$M_{total}(g) = M_t(g) + M_s(g) + M_w(g) + M_{th}(g) \tag{9}$$

E. Optical Channel Propagation Model

Light attenuation [18] is accounted as given below.

1) Absorption- The absorption is defined as the conversion of light energy into heat energy by collision. This collision is associated with the molecules of water, salt, chlorophyll and other organic compounds. Here, $a(\lambda)$ denotes coefficient of absorption, λ represents the optical beam's wavelength.

2) Scattering-This occurs when particulate particles, salt ions are dissolved in water, $b(\lambda)$ depicts scattering coefficient [19]. Underwater optical beam extinction coefficient $c(\lambda)$ by considering absorption and scattering is expressed in equation(10).

$$c(\lambda) = a(\lambda) + b(\lambda) \tag{10}$$

Where, $c(\lambda)$ is the beam extinction coefficient data for calculating propagation loss factor $l(f,\lambda)$ as given in equation (11).

$$l(f,\lambda) = exp(-c(\lambda)f) \tag{11}$$

Given, $L_{op}(f,\lambda)$ denotes total optical path loss and it is calculated as in equation (12).

$$L_{op}(f,\lambda) = \frac{S_r m_t m_r\,cos\,\theta}{2\pi\,f^2(1-cos\,\theta_0)} \cdot exp(-c(\lambda)f) \tag{12}$$

S_r implies receiver aperture, m_t and m_r represents optical efficiencies of transmitter and receiver, θ denotes inclination angle among transmitter and receiver and θ_0 denotes beam divergence angle of transmitter. The entire optical channel attenuation $J_{op}(f,\lambda)$ is represented as equation (13).

$$J_{op}(f,\lambda) = \alpha_{op}^2 \cdot L(f,\lambda) \tag{13}$$

α_{op}^2 denotes optical fading amplitude because of water turbulence. To model this, LN distribution including probability distribution function is used as given in equation (14).

$$g(\alpha) = \frac{1}{\alpha\sqrt{2\pi\sigma_Y^2}} \cdot exp\left(-\frac{(ln(\alpha)-\mu_Y)^2}{2\sigma_Y^2}\right) \tag{14}$$

A random variable Y signifies log-amplitude fading follows Gaussian distribution using mean μ_Y, variance σ_Y^2 [20], [21], [22].

Fading distributions are mainly used to replicate the random fluctuations in received signal strength in the case of an optical link, particularly when the turbulence is present. Because of its good approximation of intensity changes and mathematical tractability, the LN model is frequently employed for weak-to-moderate turbulence [2], [18], [20]. However, to represent complex turbulence environments, recent research used the GG model which captures both small- and large-scale scattering effects for moderate-to-strong turbulence [19] and the λ-k-μ distribution which offers more flexibility in describing complex fading circumstances [25].

F. Optical Noise Model

The underwater optical signals are vulnerable to a variety of disturbances to route loss caused by absorption and scattering [23]. The noise types are categorized,[11] as follows:

1) Thermal/Johnson noise- Noise variance is formulated as given in equation (15).

$$\alpha_{TH}^2 = \frac{4k_B \cdot Y_e \cdot G \cdot B}{T_L} \tag{15}$$

Where, k_B denotes Boltzmann constant $(1.38 \times 10^{-23} J/K)$, Y_e equals 290 K, G=4 is the noise figure of the system, B denotes electron bandwidth. Term T_L represents resistance of load.

2) Dark current noise- The dark current flows through the reversed-biased photodetector. It is formulated in equation (16).

$$\sigma_{DC}^2 = 2q \cdot I_{DC} \cdot B \tag{16}$$

q equals $(1.602 \times 10^{-19}\ C)$, which is the electron charge. I_{DC} equals $(1.23 \times 10^{-9} A)$ which is photo diode dark current.

3) Quantum/ Signal shot noise- Resulting from photon number at random shifts in the receiver. It is expressed in equation (17).

$$\sigma_{SS}^2 = 2q \cdot \rho \cdot Q_i \cdot B \tag{17}$$

ρ implies photo diode responsivity whereas Q_i implies signal power.

4) Background noise- All the Noise generated by ambient [24] conditions which include radiation from black body and the solar noise. It is expressed in equation (18).

$$\sigma_{BG}^2 = 2q \cdot \rho \cdot Q_{BG} \cdot B \tag{18}$$

Here, Q_{BG} is the background noise power. Thus, it is given in equation (19).

$$Q_{BG} = Q_{solar} + Q_{blackbody} \tag{19}$$

Where, Q_{solar} can be written as given equation (20).

$$Q_{solar} = S_r \cdot \pi\ (FoV)^2 \cdot \Delta\lambda \cdot Y_F \cdot A_{sol} \tag{20}$$

Where, S_r signifies receiver aperture, FoV denotes receiver field view, $\Delta\lambda$ represents optical filter bandwidth, Y_F denotes optical transmissivity and A_{sol} implies solar radiance. Thus, it is given in equation (21).

$$Q_{blackbody} = \frac{2hu^2\alpha_r \cdot \pi (FoV)^2 \cdot S_r Y_A Y_F \Delta\lambda}{\lambda^5 \cdot \left[exp\left(\frac{hc}{\lambda kT}\right) - 1\right]} \tag{21}$$

Where, Plank's constant h =$(6.62 \times 10^{-34}\ J\ S)$, u represents light velocity in water $(2.25 \times 10^8 m/s)$, α_r signifies factors of radiant absorption (0.5), Y_A implies water transmission ($Y_A = exp\ (-\tau_0)$), here τ_0 is the atmospheric transmission. Finally, λ signifies the wavelength of the light beam. In underwater optical communication, blackbody radiation noise represents the background infrared noise emitted by the environment modeled as radiation from such a theoretical blackbody. The noise sources are modeled as AWGN [25]. Total optical noise is given in equation (22).

$$\sigma_{total}^2 = \sigma_{TH}^2 + \sigma_{DC}^2 + \sigma_{SS}^2 + \sigma_{BG}^2 \tag{22}$$

The analysis done in our work has followed the channel propagation and noise models given in [11].

IV. Modulation and Coding for Optical and Acoustic Channels Setup

Quadrature Amplitude Modulation (QAM) is used in optical communication because of its capacity to deliver high data rates while remaining spectrally efficient, making it perfect for short-range, high-bandwidth underwater networks. Turbo Codes are integrated for forward error correction to mitigate the impact of absorption and scattering effects and ensure reliable data transfer. They provide both strong error recovery capabilities and low decoding latency. In contrast, for acoustic communication, the system employs Frequency Shift Keying (FSK), which is suited to acoustic transmission because of the robustness against multipath propagation, Doppler shifts and ambient noise. To enhance reliability in the presence of burst errors and fluctuating channel conditions, Reed-Solomon (RS) coding is utilized, providing powerful error correction with manageable redundancy overhead [26]. Table III shows the context aware modulation and error correction strategy.

TABLE III
CONTEXT-AWARE MODULATION AND ERROR CORRECTION STRATEGY

Mode	Modulation	Error Correction Code	Condition
Optical	QAM	Turbo Code	SNR>threshold, short distance, high traffic
Acoustic	FSK	Reed-Solomon Code	SNR low, long range, variable traffic

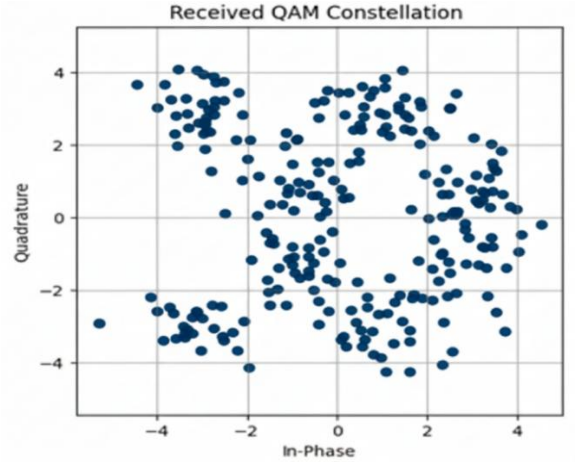

Fig. 4. QAM Constellation

Figure 4 shows the received constellation diagram for a QAM-modulated signal. The received points in this diagram are distributed around ideal positions because of noise, distortion, and underwater channel damage. Constellation clusters around coordinates like (±3, ±3) are well-defined, indicating that the QAM technique performs dependably even in moderate noise. However, as SNR declines, the spread of points grows, causing overlaps between nearby clusters and making symbol recognition more error prone. This demonstrates that, while QAM is successful for high-data-rate underwater optical communication, maintaining a high link quality is critical for reducing bit mistakes and ensuring precise demodulation.

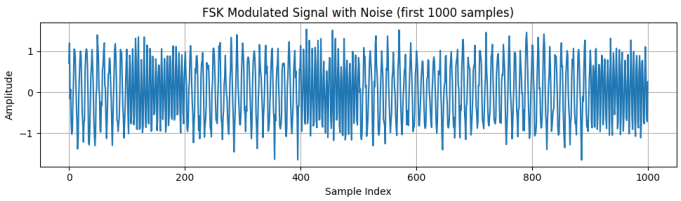

Fig. 5. FSK Modulated Wave

Figure 5 illustrates a segment of an FSK modulated acoustic signal corrupted by underwater channel noise. This shows its robustness in noisy underwater acoustic channels, as frequency shifts are easier to detect than amplitude or phase changes under noise. This supports the choice of FSK for long-range acoustic communication where noise and multipath effects are significant.

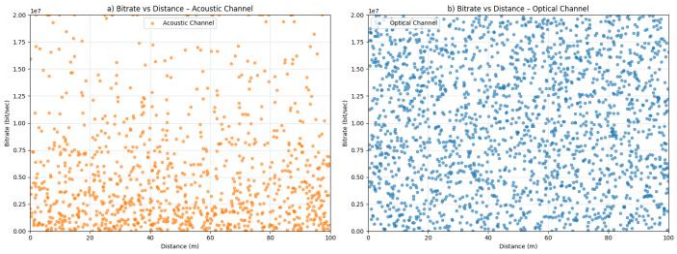

Fig. 6. a) Bit rate vs Acoustic Distance b) Bit rate vs optical Distance

Figure 6(a) illustrates the relationship between bit rate and acoustic transmission distance. As the acoustic distance increases from 0 to 100 meters, a noticeable dispersion in bit rates is observed, indicating reduced communication reliability over longer distances. While a few transmissions manage to maintain higher bit rates even at extended ranges, a significant clustering of data points at lower bit rates highlights the impact of increased bit errors due to factors such as attenuation, multipath propagation, and ambient underwater noise. In Figure 6(b) we see the bit rate versus optical distance plot. In contrast to acoustic channels, the optical channel demonstrates a relatively stable distribution of bit rates across short to moderate distances (0 to 100 meters), particularly within the effective operational range (typically under 10 meters).

V. Optimization using Electric Eel Foraging Optimization Algorithm (EEFOA)

EEFOA is used to allocate transmission power efficiently. Its inspired adaptive behavior effectively strikes a balance between exploitation and exploration, leading to higher solution accuracy and faster convergence. EEFOA dynamically adjusts to shifting network circumstances resulting in increased energy efficiency and less interference among transmitting nodes. Its robustness in handling nonlinear, multi objective optimization problems makes it ideal for complicated wireless communication environment resulting in optimal resource use and extended network lifetime [27]. The entire step method is presented as given below.

Step 1: Initialization

In the EEFOA initialization phase, eel positions are produced at random between the design variable boundaries is represented in equation (23).

$$S = \begin{bmatrix} S_{11} & S_{12} & \dots & S_{1D} \\ S_{21} & S_{22} & \dots & S_{2D} \\ \vdots & \vdots & \ddots & \vdots \\ S_{N1} & S_{N2} & \dots & S_{ND} \end{bmatrix}_{N\times D} \quad (23)$$

where, S is a matrix of size $N \times D$, where N signifies population size, D shows dimension of design variables.

Step 2: Random Generation

In this step, input parameters are randomly generated while strictly following the defined hyperparameters requirements for model consistency and effective tuning.

Step 3: Fitness Function

It makes random solutions from initialization. This is assessed by exploration node.

$$FitnessFunction = Optimizing[TransmissionPowerAllocation] \quad (24)$$

The weight of each electric eel corresponds to its normalized fitness value, ensuring that individuals closer to the global optimum have a stronger influence on search dynamics. Specifically, we use an inverse-fitness normalization as given by,

$$w_i = \frac{1/fit_i}{\sum_{j=1}^{n} 1/fit_j} \quad (24a)$$

Where fit_i is the objective function of eel i, and N is the population size.

Step 4: Interacting

At an approach to a school of fish, the eels swim together, thereby establish a circular structure to capture food in the middle. The optimal solution at all stages is regarded as intended prey in EEFO, where each eel stands for a potential solution. Eels cooperatively interact using position information enabling global exploration. An eel can randomly interact with any other eel in population, utilizing collective position data. Position updates are determined by comparing difference among randomly selected eel, population center. It is given as,

$$y_r = Low + t(Up - Low) \quad (25)$$

Here, y_r denotes size of the population, t denotes random vector with [0, 1], Up and Low signifies lower, upper boundaries. Electric eels can migrate towards various locations in the search space to their interactive behaviour which can greatly aid in investigation of EEFO throughout search environment.

Step 5:Resting

In EEFOA, there is a need to establish a prior resting area. For that a region where dimensions of eel's position vector are anticipated into main diagonal at search space to increase search efficiency. Both search spaces and eel's location are normalised to 0-1 range to position resting place for eel. The search space's major diagonal is then projected with randomly chosen location values. The anticipated position represents an eel's resting area middle. It is given in equation (26).

$$\{Y|Y - X(y)| \leq \alpha_{EEFO} \times |X(y) - y_{prey}(y)\} \quad (26)$$

Here, y_{prey} signifies position vector of optimal solutions attained so far, α_{EEFO} signifies an initial resting area scale, X implies a normalized number and Y denotes position selected at random from existing populace. An eel adjusts its location toward a resting region based on its location. This location will be inside the area [27]. An energy factor regulates search behaviors in EEFOA and is described by,

$$E(t) = 4 \times sin(1 - t/T) \times ln(1/r) \quad (27)$$

Here, a random number r is taken within (0,1) with total number of iterations as T. If E(t) is greater than 1, eels search in a global space resulting in an exploration. Otherwise, it will be an exploitation.

Step 6: Hunting

The eels form a coordinated circular pattern around while detecting prey; they do not swarm; throughout this process, the electrified circle gradually shrinks, driving the prey toward shallower waters where capture is easier. The circle serves as the area for hunting thereby the prey will panic and make unpredictable movements within the confined space. Consequently, the prey rapidly shifts positions within the

hunting space due to fear and disorientation. It is given in equation (28).

$$J_{prey}(t+1) = y_{prey}(t) + \beta_{EEFO} \times \left|\bar{y}(t) - y_{prey}(t)\right| \quad (28)$$

$\bar{y}(t)$ represents initial scale of hunting area, J_{prey} denotes novel prey position concerning its previous location in hunting area, y_{prey} denotes eel centers on the prey, and β_{EEFO} denotes the shrinking of the hunting area with the progress. An eel's posture is changed to reflect altered location of its prey through curling movement, which is a hunting behaviour seen in EEFO. It is given as below.

$$b_i(y+1) = J_{prey}(y+1) + \eta \times \left(J_{prey}(y+1) - round(rand) \times y_i(y)\right) \quad (29)$$

Here, η indicate the curling factor, hunting behaviour of eel involves encircling its prey, during which red dots mark the position footprints of the prey as it performs swan dive. At this stage, the eel employs a curling motion to shock the prey, and the recorded position footprint is utilized to update eel's location in next iteration.

Step 7: Migrating

Eels frequently relocate from their rest area to regions of hunting. The migration behavior is written as.

$$L = 0.01 \times \left|\frac{u \cdot \sigma}{b_{ee}^{\frac{1}{b_{ee}}}}\right| \quad (30)$$

Here, L denotes Levy flight function, it is offered during EEFO exploitation phase to prevent being trapped in local optima, b_{ee} represents a migration shape parameter, σ represents considered any location within hunting area.

The computational complexity of EEFOA is affected by the number of individual electric eels, the dimensional variables, and the number of iterations made. We can summarize the total computational complexity as given by the equation (31).

$$C(EEFO)=C(Problem\_definition)+C(Initialization)+C(Evaluation)+C(Postion\_updating\_interating+C(Postion\_updating\_resting)+C(Postion\_updating\_migrating)+C(Postion\_updating\_hunting) \quad (31)$$

Step 8: Termination

EEFOA iteratively adjusts power levels until a halting criterion such as convergence in energy usage or reaching a predefined number of iterations is met [27]. Table IV shows the parameter settings used for configuring the EEFO algorithm.

TABLE IV
EEFO PARAMETER SETTINGS

Parameter	Values
Population	20
Dimension	1
Lower bound	0.1
Upper bound	1.0
Iterations	50

VI. RESULTS AND DISCUSSION

The simulation outcomes of our work are discussed in this section which includes analysis and evaluation of energy consumption, throughput, normalized mean traffic load, received load, and average power savings.

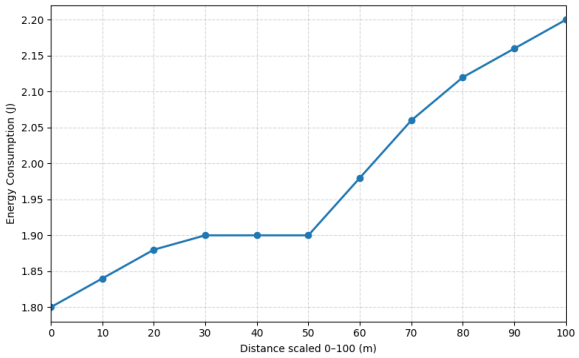

Fig. 7. Energy vs Distance

Figure 7 shows the relationship between energy consumption (in joules) and distance (scaled from 0 to 100) in an underwater wireless communication scenario. As the distance increases, energy consumption rises gradually from 1.8 J at the shortest distance, with a slight plateau between distances 30 and 50, indicating stable energy usage in that range. Beyond 50, energy consumption increases more sharply, reaching about 2.2 J at the maximum distance. This trend reflects the higher power required for reliable data transmission over longer underwater distances, likely due to greater signal attenuation and noise, which necessitate increased transmission power or more robust error correction mechanisms.

The EEFOA optimizer's convergence was monitored using the best global fitness value over iterations. Convergence is obtained in approximately about 35 iterations, demonstrating the algorithm's monotonic improvement and stability at an approximately population size of N = 50. After 40 iterations, the fitness standard deviation across runs falls below 2 %, demonstrating robustness.

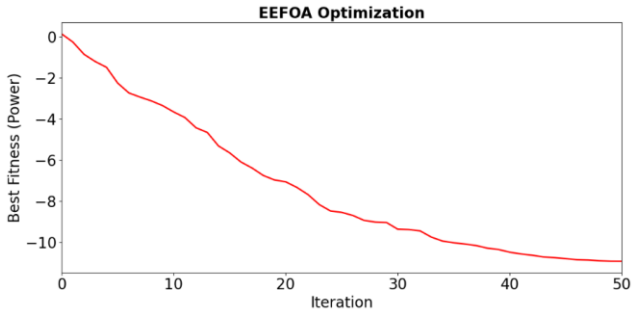

Fig. 8. EEFOA optimization

EEFOA Performance

A performance comparison of EEFOA is done with Genetic Algorithm (GA) and particle Swarm Optimization (PSO) by applying the same parameters of simulation with population of 20, dimension of 1 and a bound given as [0.1, 1.0]. In contrast to PSO and GA, which require 27 and 41 iterations, respectively, EEFOA converges far more quickly, requiring just 12 iterations to attain 95% of the ideal value, as shown in Table V. Additionally, EEFOA achieves the shortest calculation time and the lowest final energy consumption. It is especially useful for hybrid optical–acoustic links because of its electro-sensory hunting behavior combined with exploitation around the best candidates.

TABLE V
COMPARISON OF EEFOA, PSO AND GA

Algorithm	Convergence Speed	Final Energy (J)	Computation Time (s)
EEFOA	12	0.142	0.018
PSO	27	0.158	0.024
GA	41	0.165	0.031

Performance Analysis

Figure 9 depicts performance analysis of the proposed model. These findings support the proposed model's efficiency, attributed to its hybrid approach and dynamic decision based on distance and channel circumstances. Figure 9(a) depicts the relationship between energy and acoustic distance, with the energy fluctuating between approximately 86 J and 96 J as the acoustic distance increases from 50 to 200 m. The energy fluctuations follow a shifting pattern that is typical of acoustic signal propagation over increasing distances, with the energy remaining within a relatively wide range. From 9(b) the relationship between energy and optical distance can be observed. The energy rises with optical distance. Compared to the acoustic scenario, the energy fluctuations for optical propagation are significantly smaller. 9(c) depicts the relationship between throughput and acoustic distance. After 150 m, throughput fluctuates. The system's performance varies greatly over distances, revealing that acoustic channel conditions have a substantial impact on throughput, highlighting the necessity for adaptive techniques to enhance performance.

The variation in throughput with optical distance is visible in 9 (d). Despite variations, the optical communication system regularly outperforms the acoustic method, with a peak performance of over 33.3 kbps. However, like the acoustic system, optical communication performance diminishes at a given distance, possibly due to attenuation or scattering effects. Normal load versus acoustic distance is plotted in Figure 9(e). As we see, large and frequent swings in normalized load indicate that the conditions of the acoustic channel, such as signal quality and interference, have a major impact on the system's load management capability. 9(f) depicts the normalized load for optical communication, as can be seen, the oscillations are substantially lower than those seen with the acoustic method, demonstrating that optical communication is more efficient at handling data load. The narrower range and peak at 150m indicate that optical communication systems are well-suited for load control at this distance, most likely due to their larger bandwidth capacity and more efficient data processing. The fluctuation in average power required for acoustic communication as acoustic distance increases is shown in 9(g). It shows that the power requirements for acoustic communication are very dynamic and dependent on distance and channel conditions. The variability shows that adaptive power management is critical for maximizing energy consumption while maintaining communication quality. 9(h) displays the average power required for optical communication. These values are orders of magnitude lower than those for acoustic communication. The optical system has little change in power and exhibits tiny dips and climbs in the first segment. Despite these variations, optical communication has substantially lower power requirements than auditory transmission, showing the energy economy of optical networks. 9(i) shows the Packet Delivery Ratio (PDR) for acoustic communication over various distances. Despite the fluctuations, the system maintains a high PDR, suggesting that sound communication is effective yet extremely sensitive to environmental or distance-related variables. This emphasizes the significance of error correcting technologies in underwater communication systems to ensure reliability. 9(j) depicts the PDR for optical communication with values lower than the acoustic PDR and have smaller fluctuations. Although the optical communication system does not approach the higher PDRs reported in acoustic communication, it has more constant performance with less dramatic variations. This suggests that although optical links offer stable packet delivery, higher losses occur over longer distances due to the scattering and absorption factors.

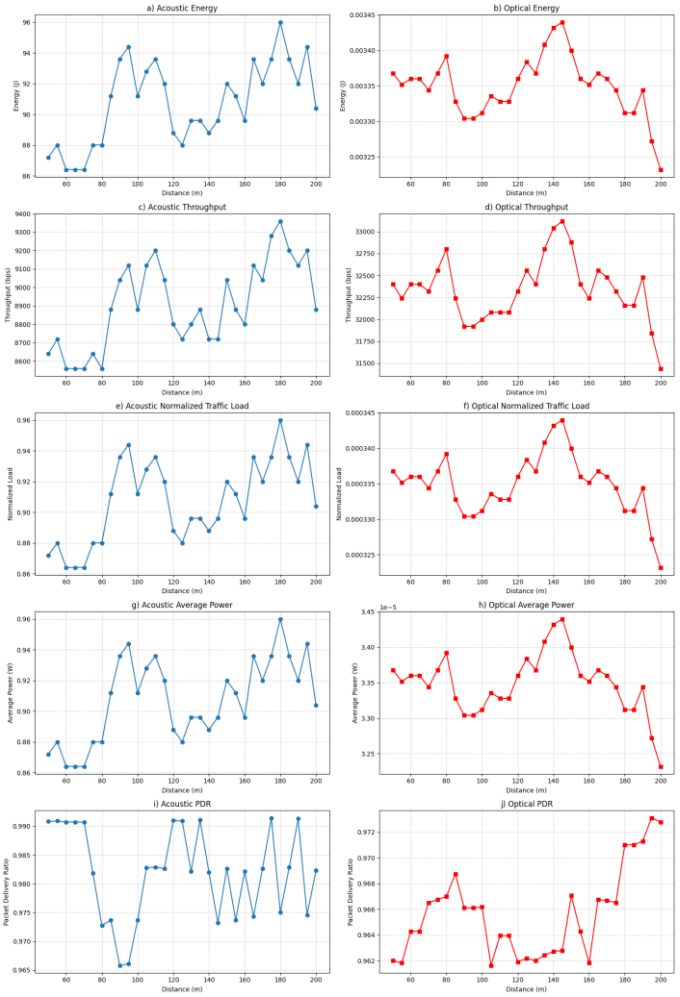

Fig. 9. Performance analysis

VII. CONCLUSION AND FUTURE SCOPE

This work presents a hybrid underwater communication framework that integrates optical and acoustic transmission modes with joint modulation and channel coding strategies. To improve energy efficiency, a bio-inspired Electric Eel Foraging Optimization algorithm was used for transmission power optimization. Simulation results demonstrated that the proposed hybrid framework significantly reduces energy consumption while improving throughput and communication reliability. The results confirm that combining optical and acoustic links with

joint modulation and intelligent power allocation can effectively overcome the inherent trade-offs between bandwidth, range, and energy efficiency in underwater environments.

Future research will extend this work by incorporating learning-based adaptive mode selection and uncertainty-aware decision mechanisms to dynamically switch between optical and acoustic links under stochastic underwater channel conditions. Neural network models shall be explored to quantify prediction uncertainty and improve robustness in unpredictable environments. A separate study will also investigate data-driven channel-aware hybrid communication architectures using realistic training–testing partitioning and stochastic fading realizations. These extensions will be useful to have a more comprehensive and practical hybrid underwater communication framework suitable for real-time autonomous underwater systems.

Additionally, future research will focus on validating the proposed framework in realistic underwater testbeds and integrating real-time environmental sensing to dynamically adapt modulation and power allocation under changing channel conditions Use of channel simulators and multipath-aware propagation models will further enhance system realism.

REFERENCES

[1] W. Zhu, X. Zeng, and Y. Qiu, "A Routing Protocol for Underwater Acoustic-Optical Hybrid Wireless Sensor Networks Based on Packet Hierarchy and Void Processing," IEEE Sens. J., vol. 24, no. 4, pp. 5203–5214, Feb. 2024, https://doi.org/10.1109/JSEN.2023.3348757

[2] Z. Zeng, S. Fu, H. Zhang, Y. Dong, and J. Cheng, "A Survey of Underwater Optical Wireless Communications," IEEE Communications Surveys and Tutorials, vol. 19, no. 1. Institute of Electrical and Electronics Engineers Inc., pp. 204–238, Jan. 01, 2017, https://doi.org/10.1109/COMST.2016.2618841

[3] O. Bello and S. Zeadally, "Internet of underwater things communication: Architecture, technologies, research challenges and future opportunities," Ad Hoc Networks, vol. 135, no. July, 2022, https://doi.org/10.1016/j.adhoc.2022.102933

[4] M. C. Domingo, "An overview of the internet of underwater things," J. Netw. Comput. Appl., vol. 35, no. 6, pp. 1879–1890, 2012, https://doi.org/10.1016/j.jnca.2012.07.012

[5] Y. Guo et al., "Current Trend in Optical Internet of Underwater Things," IEEE Photonics J., vol. 14, no. 5, Oct. 2022, https://doi.org/10.1109/JPHOT.2022.3195700

[6] Z. Qu and M. Lai, "A Review on Electromagnetic, Acoustic, and New Emerging Technologies for Submarine Communication," IEEE Access, vol. 12, pp. 12110–12125, 2024, https://doi.org/10.1109/ACCESS.2024.3353623

[7] C. M. G. Gussen, P. S. R. Diniz, M. L. R. Campos, W. A. Martins, F. M. Costa, and J. N. Gois, "A Survey of Underwater Wireless Communication Technologies," J. Commun. Inf. Syst., vol. 31, no. 1, pp. 242–255, 2016, https://doi.org/10.14209/jcis.2016.22

[8] M. Jahanbakht, W. Xiang, L. Hanzo, and M. R. Azghadi, "Internet of Underwater Things and Big Marine Data Analytics - A Comprehensive Survey," IEEE Commun. Surv. Tutorials, vol. 23, no. 2, pp. 904–956, 2021, https://doi.org/10.1109/COMST.2021.3053118

[9] H. Luo, Z. Xu, J. Wang, Y. Yang, R. Ruby, and K. Wu, "Reinforcement Learning-Based Adaptive Switching Scheme for Hybrid Optical-Acoustic AUV Mobile Network," Wirel. Commun. Mob. Comput., vol. 2022, 2022, https://doi.org/10.1155/2022/9471698

[10] J. Cao, J. Dou, L. Chu, C. Qu, L. Wang, and B. Zhao, "Optimum Data Transmission Allocation in Multimodal Communication of Underwater Sensor Networks," IEEE Commun. Lett., vol. 26, no. 4, pp. 788–792, 2022, https://doi.org/10.1109/LCOMM.2021.3090669

[11] K. Y. Islam, I. Ahmad, D. Habibi, M. I. A. Zahed, and J. Kamruzzaman, "Green Underwater Wireless Communications Using Hybrid Optical-Acoustic Technologies," IEEE Access, vol. 9, pp. 85109–85123, 2021, https://doi.org/10.1109/ACCESS.2021.3088467

[12] B. R. Angara, P. Shanmugam, and H. Ramachandran, "Underwater Wireless Optical Communication System Channel Modelling With Oceanic Bubbles and Water Constituents Under Different Wind Conditions," IEEE Photonics J., vol. 15, no. 2, Apr. 2023, https://doi.org/10.1109/JPHOT.2023.3258500

[13] J. Zhang et al., "Long-Term and Real-Time High-Speed Underwater Wireless Optical Communications in Deep Sea," IEEE Commun. Mag., vol. 62, no. 3, pp. 96–101, Mar. 2024, https://doi.org/10.1109/MCOM.001.2300461

[14] S. A. A. El-Mottaleb, M. Singh, A. Atieh, and M. H. Aly, "OCDMA transmission-based underwater wireless optical communication system: performance analysis," Opt. Quantum Electron., vol. 55, no. 5, May 2023, https://doi.org/10.1007/s11082-023-04742-8

[15] A. Celik, N. Saeed, B. Shihada, T. Y. Al-Naffouri, and M. S. Alouini, "A Software-Defined Opto-Acoustic Network Architecture for Internet of Underwater Things," IEEE Commun. Mag., vol. 58, no. 4, pp. 88–94, Apr. 2020, https://doi.org/10.1109/MCOM.001.1900593

[16] M. Stojanovic and J. Preisig, "Underwater Acoustic Communication Channels: Propagation Models and Statistical Characterization," IEEE Commun. Mag., vol. 47, no. 1, pp. 84–89, 2009, https://doi.org/10.1109/MCOM.2009.4752682

[17] L. J. Johnson, "The Underwater Optical Channel," https://doi.org/10.13140/RG.2.1.1295.7283

[18] S. K. Sahu and P. Shanmugam, "A theoretical study on the impact of particle scattering on the channel characteristics of underwater optical communication system," Opt. Commun., vol. 408, no. May 2017, pp. 3–14, 2018, https://doi.org/10.1016/j.optcom.2017.06.030

[19] Y. Li, M. S. Leeson, and X. Li, "Impulse response modeling for underwater optical wireless channels," Appl. Opt., vol. 57, no. 17, p. 4815, Jun. 2018, https://doi.org/10.1364/ao.57.004815

[20] S. Tang, Y. Dong, and X. Zhang, "Impulse response modeling for underwater wireless optical communication links," IEEE Trans. Commun., vol. 62, no. 1, pp. 226–234, 2014, https://doi.org/10.1109/TCOMM.2013.120713.130199

[21] L. Zhou, Y. Zhu, and W. Zheng, "Analysis and Simulation of Link Performance for Underwater Wireless Optical Communications," EAI Endorsed Trans. Wirel. Spectr., vol. 3, no. 12, p. 153467, 2017, https://doi.org/10.4108/eai.12-12-2017.153467

[22] R. Bhatnagar and P. Garg, "Performance analysis of hybrid underwater wireless system for shallow sea monitoring," Photonic Netw. Commun., vol. 46, no. 2–3, pp. 78–89, 2023, https://doi.org/10.1007/s11107-023-01003-2

[23] W. Cox and J. Muth, "Simulating channel losses in an underwater optical communication system," J. Opt. Soc. Am. A, vol. 31, no. 5, p. 920, May 2014, https://doi.org/10.1364/josaa.31.000920

[24] T. Hamza, M.-A. Khalighi, S. Bourennane, P. Léon, and J. Opderbecke, "Investigation of solar noise impact on the performance of underwater wireless optical communication links," Opt. Express, vol. 24, no. 22, p. 25832, 2016, https://doi.org/10.1364/oe.24.025832

[25] Z. Vali, A. Gholami, Z. Ghassemlooy, and D. G. Michelson, "System parameters effect on the turbulent underwater optical wireless communications link," Optik (Stuttg)., vol. 198, Dec. 2019, https://doi.org/10.1016/j.ijleo.2019.163153

[26] W. C. Cox, J. A. Simpson, C. P. Domizioli, J. F. Muth, and B. L. Hughes, "An underwater optical communication system implementing reed-

solomon channel coding," Ocean. 2008, pp. 1–6, 2008, https://doi.org/10.1109/OCEANS.2008.5151992

[27] W. Zhao, L. Wang, Z. Zhang, H. Fan, J. Zhang, S. Mirjalili, N. Khodadadi, and Q. Cao, "Electric eel foraging optimization: A new bio-inspired optimizer for engineering applications," Expert Syst. Appl., vol. 238, p. 122200, 2024, https://doi.org/10.1016/j.eswa.2023.122200

[28] F. Busacca, L. Galluccio, S. Palazzo, and A. Panebianco, "A comparative analysis of predictive channel models for real shallow water environments," Comput. Netw., vol. 250, p. 110557, 2024, https://doi.org/10.1016/j.comnet.2024.110557

[29] M. K. Ghosh and M. Z. Chowdhury, "Enhancing underwater acoustic communication networks with RIS: Precise performance analysis over κ–μ shadowed fading distribution," Results Eng., p. 105446, 2025, https://doi.org/10.1016/j.rineng.2025.105446

[30] M. Haziq, Q. V. Phung, S. Lachowicz, D. Habibi, and I. Ahmad, "Modulation techniques for underwater acoustic communication: A comprehensive survey," IEEE Access, vol. 13, pp. 150715-150755, 2025, https://doi.org/10.1109/ACCESS.2025.3601799